



Research paper

Resin modified MIL-53 (Fe) MOF for improvement of photocatalytic performance



Tirusew Araya^{a,b,c}, Manke Jia^{b,c}, Jian Yang^{b,c}, Ping Zhao^{b,c}, Kuan Cai^{b,c}, WanHong Ma^{b,c,*}, Yingping Huang^{a,b,c,*}

^a College of Hydraulic & Environmental Engineering, China Three Gorges University, Yichang, 443002, China

^b Innovation Center for Geo-Hazards and Eco-Environment in Three Gorges Area, Hubei Province, Yichang, 443002, China

^c Engineering Research Center of Eco-Environment in Three Gorges Reservoir Region, Ministry of Education, China Three Gorges University, Yichang, 443002, China

ARTICLE INFO

Article history:

Received 18 August 2016

Received in revised form 25 October 2016

Accepted 26 October 2016

Available online 27 October 2016

Keywords:

MIL-53(Fe)

Immobilization

Amberlite resin

Tunable degradation

Photocatalysis

ABSTRACT

Metal organic frameworks (MOFs) are fascinating materials for diverse applications due to their adjustability of aperture and structure. Herein, a three-dimensional iron-based MOF with BDC linker ($BDC = 1,4\text{-benzenedicarboxylate}$), commonly known as MIL-53(Fe), has been synthesized and successfully composited with anionic resin (Amberlite IRA 200) and cationic resin (Amberlite IRA 900) resulting solid composite photocatalysts, AMIL-53 (Fe) and DMIL-53(Fe), respectively. In the novel composite photocatalysts, bulky MIL-53(Fe) MOF solids are used as both a support to anchor the finely ground Amberlite IRA resin powders and as a visible light active component for the degradation of organic pollutants in water. In addition to being a traditional support, the resins here were used as a co-catalyst (with loading ration of the resin to MIL-53(Fe) is controlled around 20 wt%) to capture and transfer pollutant molecule from bulk solution into the active centers of the composited catalysts. Such an immobilization of the resins significantly alters MIL-53 (Fe) activity and degradation selectivity of dye pollutants; after 120 min of visible light illumination ($\lambda \geq 420\text{ nm}$) removal yield of SRB (24%) by the bare MIL-53 (Fe) was apparently improved to 96% after MIL-53 (Fe) was modified by Amberlite IRA 900, DMIL-53(Fe). The tunable degradation order was demonstrated by employing AMIL-53 (Fe) for the selective degradation of cationic dyes while DMIL-53 (Fe) for the degradation of anionic dyes. Furthermore, the composites activity was optimized by controlling resin to MOF ratio during immobilization. Immobilization also improves ease of separation and recyclability of the original MOF. Especially, AMIL-53 significantly reduces iron ion leaching resulting in an enhanced stability. The photocatalytic mechanism under visible-light irradiation is also discussed.

© 2016 Elsevier B.V. All rights reserved.

1. Introduction

Metal organic frameworks (MOFs) are a rapidly growing class of hybrid organic-inorganic supramolecular materials in which metal ion/metal oxide clusters held together in a three-dimensional structure by organic linkers. Recent researches demonstrated that under light irradiation, the organic bridging ligands can serve as antennas to harvest light and activate the metal nodes of MOFs indicating semiconductor-like behavior [1–4]. This motivates researchers to develop new MOFs-based catalytic material which utilizes solar energy for degradation of pollutants in water. The

large scale application of MOFs however is still challenging due to their stability and degradation selectivity towards target pollutants in water. Katrien et al. demonstrated the stability and physical state of MOFs that could affect their photocatalytic behavior [4]. Leaching of metal ion from the framework in water solutions is one of the challenging problems needed to be resolved. These instabilities simply limit the practical uses of MOFs [5,6].

On the other hand, selective degradation of toxic target molecules enhances catalyst efficiency and is crucial in environmental remediation. It is widely known that preferentially adsorbed molecules can react more efficiently with photogenerated active species. Electrostatic interaction, pore/size-selective, surface molecular imprinting technique, acid-base interaction, hydrogen bonding, $\pi-\pi$ interactions, and hydrophobic interaction are the main driving force in selective adsorption of pollutants on

* Corresponding authors at: Innovation Center for Geo-Hazards and Eco-Environment in Three Gorges Area, Hubei Province, Yichang, 443002, China.

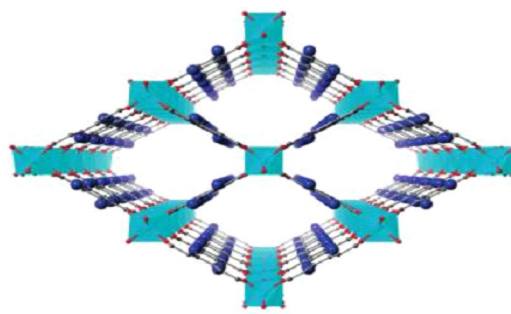
E-mail addresses: whma@iccas.ac.cn (W. Ma), chem.ctgu@126.com (Y. Huang).

adsorbents [7–9]. In general, MOFs mainly show pore size- and charge-based selectivity [10]. However, it is not easy to accommodate relative big molecule since most MOFs contain pores with less than 2 nm diameter [11]. Moreover, a series of positively charged MOFs developed demonstrates highly selective ion exchange process for negatively charged substrates [12]. However, charge based selective MOFs are directional and their desirable photocatalytic activity is less significant if they experience repulsive Columbic interaction with the target pollutant. So it is highly desirable to tune the selectivity of MOFs without affecting their desirable photocatalytic behavior.

Immobilization on inert carriers is a promising approach to enhance recyclability, stability and selectivity [13]. Recently, MOFs have been immobilized on supports such as fiber glass [14], silica [15] and graphene [16] to enhance stability and photocatalytic activity. Graphene oxide (GO) has also been widely utilized as a support and shows to improve the stability and optical properties of MOFs [17,18]. However, GO membrane blocks large organic dyes and the magnitude of its electrostatic attraction due to its negative charge is too small to afford a significant selective adsorption [19].

Ion exchange resins have attracted research interest as a catalyst support for their stability, high adsorption capacity and rapid kinetics [6,20]. Resins are economical, ecofriendly, stable, versatile, and can easily be separated from the reaction mixture [21]. The functional groups are crucial in substrate adsorption and desired surface polarity can be achieved through modification of functional moieties [22,23]. Resins are also capable of chelating metal ions depending on surface exposed terminal electronegative groups [24,25]. Metallophthalocyanines immobilization on anion exchange resin enhances adsorption capacities and recyclability [26]. Cation exchange resins also induce heterogeneity to water soluble iron ions due to electrostatic interaction between the metal ions and negatively charged sulfonated functional groups [27,28]. For instance, immobilization of water soluble photo-inactive $\text{Fe}(\text{bpy})_3^{2+}$ over a cation exchange resin generates a heterogeneous photocatalyst [29]. Feng et al. loaded cyclometalated Pt (II) complex $\text{Pt}(\text{L})\text{Cl}$ on a cation-exchange resin Amberlite IRA-200. Interestingly, very low (0.54 wt%) loading of the Pt complex showed to be effective in photodegrading organic pollutants [30]. Even though Amberlite IRA-900 does not affect the typical photocatalytic activity of anchored photocatalyst centers such as, $\text{W}_{10}\text{O}_{32}^{4-}$, the anionic exchange resin plays a crucial role in fostering the enrichment of anionic species close to the surface thereby significantly increasing their reaction efficiency with the photo-generated active species [26]. Nonetheless, as a classic support, the ion-exchange resin is always used to anchor different active components rather than it is loaded on the active component body so far.

MIL-53(Fe) is a three-dimensional porous solid built up by infinite one-dimensional linkage of $-\text{Fe}-\text{O}-\text{O}-\text{Fe}-\text{O}-\text{Fe}-$, cross-linked by bis-bidentate terephthalate(1,4-benzenedicarboxylate) linkers as shown in Scheme 1. Very recently, MIL-53(Fe) solids are selected as the target photocatalyst owing to its low cost, nontoxic nature and visible light response. Bare MIL-53(Fe) has also exhibited considerable adsorption and photocatalytic activity for the treatment of wastewater, which makes it a potential candidate for environmental restoration [31,32]. However, directly suspending MIL-53(Fe) in water to serve as a photocatalyst for the degradation of non-biodegradable organic pollutants never grows to its optimal levels. Especially, the degradation of anionic pollutants in water by MIL-53 (Fe) is generally very poor, because of its rich carboxyl ligands that prevent these organic pollutants with anionic groups from approaching catalytic sites. There is an urgent need to modification of MIL-53 (Fe) so as to enhance its ability of approaching to and decomposing not only cationic but also anionic pollutants in water.



Scheme 1. The Schematic 3D representation of MIL-53 (Fe). Reprinted with permission from Shigematsu et al. [36].

In this work, anionic (Amberlite IRA 200) and cationic (Amberlite IRA 900) resins were allowed to be immobilized over solid MIL-53 (Fe) as visible-light photocatalyst for the degradation of either cationic or anionic dye pollutants in water. The finely ground resin powders are used as co-catalyst, while bulky solid MIL-53(Fe) MOF is used as both an active center and a support. The ratio (wt%) of the resin to MIL-53(Fe) in the composite photocatalyst is controlled around 20%. Amberlite IRA 200 and Amberlite IRA-900, with strongly acidic sulfonyl groups and strongly basic quaternary ammonium groups, respectively, are macroreticular polystyrene-based ion exchange resins which have been used to support several catalysts [25,26]. In general, the activity of catalysts more or less decreases once immobilized to supports, while makes it easier for the recycle of catalysts. On the contrary, immobilization do not lower MIL-53(Fe) activity, instead significantly increase its activity and improve its discernable degradation capacity and stability when degrading organic dye pollutants in water under visible light irradiation. Our results provide a new view to re-examine the immobilization effects on activity and highlight the feasibility and practicality of novel immobilization strategy in waste water treatment.

2. Experimental

2.1. Materials and reagents

Rhodamine B (RhB), methylene blue (MB), orange II (Org II) and sulphorhodamine B (SRB) were of analytical grade and were used without further purification. Amberlite IRA 200 and Amberlite IRA 900 were obtained from Nankai University, China. 1,4-benzene dicarboxylic acid, iron(III) chloride hexahydrate ($\text{FeCl}_3 \cdot 6\text{H}_2\text{O}$), N,N'-dimethylformamide (DMF), Benzoquinone ($\text{C}_6\text{H}_4\text{O}_2$), sodium azide (NaN_3), ammonium oxalate ($\text{NH}_4\text{C}_2\text{O}_4$) and isopropyl alcohol ($\text{C}_3\text{H}_8\text{O}$) were purchased from Sigma-Aldrich. All other reagents used in this study were of analytical grade. Deionized water was used throughout this study. Aqueous solutions of HCl and NaOH were used to adjust the pH. XRD patterns were carried out on a D/max2500 (Rigaku) X-ray diffractometer operated at 40 kV and 40 mA with $\text{Cu K}\alpha$ irradiation ($\lambda = 0.15406 \text{ nm}$). The data were recorded in the 2θ range of 5–50°. UV-vis diffuse reflectance spectra (UV-vis DRS) were obtained by a Shimadzu UV-3100 spectrophotometer with BaSO_4 as a reflectance standard. X-ray photoelectron spectroscopy (XPS) measurements were conducted on a VG Multilab 2000 XPS system equipped with an Al X-ray source. FT-infrared (FT-IR) spectra were carried out on a Nicolet iS 50 Fourier transform infrared spectrometer. The morphologies of the different samples were characterized by using a scanning electron microscope JSM-7500F field SEM. The zeta potentials of samples in aqueous solution were determined using a ZEN3690 (Malvern Instruments).

2.2. Preparation of composite photocatalysts

MIL-53 (Fe) was synthesized using solvothermal method as previously reported [32], a mixture of terephthalic acid (H_2BDC , 5 mmol), iron (III) chloride hexahydrate ($FeCl_3 \cdot 6H_2O$, 5 mmol) and N,N'-dimethylformamide (DMF, 1.4 mol) was transferred to a Teflon-lined pressure vessel heated at 150 °C for 15 h. The suspension was filtered and washed with deionized water and dried at 150 °C for 12 h to afford MIL-53 (Fe). Before being used to modify MIL-53 (Fe), the resins were washed with 1 M HCl and 1 M NaOH repeatedly and then with water until the effluents were transparent in the UV region. To increase the surface area and improve adsorption, the resins were ground to powder. Immobilization was carried out by stirring the resins in an aqueous suspension of MIL-53 (Fe) overnight. The supernatant was removed by filtration and the resulting products, AMIL-53 (Fe) and DMIL-53 (Fe), were air dried. The resins were immobilized on MIL-53 (Fe) in various weight proportions (10%, 20%, 30%, 40% by wt%)

2.3. Photoreactor and light source

The photocatalytic activity and selectivity of the catalysts under visible light irradiation were examined by degrading organic dyes, Rhodamine B (RhB), Methylene blue (MB), orange II (Org II) and Sulphorhodamine B (SRB) in a 75 mL test tube at room temperature, open to air. The reaction was irradiated by a 400 W Xe lamp with a 420 nm cutoff filter. The distance between the light source and reaction vessel was fixed at 10 cm prior to irradiation, the suspension was magnetically stirred in the dark for 1 h to ensure the adsorption/desorption equilibrium was established and a magnetic stirrer was used to keep the photocatalyst suspended. Samples were withdrawn at regular time interval and immediately centrifuged to prepare the solution for analysis. Dye concentration in centrifugal liquids was appropriately diluted and then was determined by running a full scan UV-vis spectrophotometer (200–700 nm) with a 1 cm quartz cell.

2.4. Detection of leached iron from AMIL-53 (Fe), DMIL-53 (Fe) and MIL-53(Fe)

500 μ L of 0.1 g mL^{-1} hydroxylamine hydrochloride was added into 500 μ L of the supernatant that was separated from 5 mg mL^{-1} AMIL-53 (Fe), DMIL-53 (Fe) and MIL-53(Fe) solution, respectively, and 100 μ L of 1.5 mg mL^{-1} 1,10-phenanthroline monohydrate was added into the above mixing solution. The absorbance of the mixing solution was measured at 508 nm [33].

3. Results and discussion

3.1. Characterization

MIL-53(Fe) is a three-dimensional porous solid where the metal clusters are cross-linked by terephthalic acid linkers creating a three dimensional framework with a one-dimensional pore channel system [32–35].

The morphological analysis of the resins and the as-synthesized composite photocatalysts were conducted by scanning electron microscopy (SEM) as shown in Fig. 1. As can be seen from Fig. 1a and b, both Amberlite IRA 200 and Amberlite IRA 900 respectively display spherical and compacted structures. In contrast, the SEM image of MIL-53 (Fe) (Fig. 1c) shows well crystallized rod like structures. The introductions of both resins bring a significant change in the surface morphology of the original MOF. The SEM images of the resulting composites AMIL-53 (Fe) (Fig. 1d) and DMIL-53 (Fe) (Fig. 1e) show an intimate interfacial contact between the block

MIL-53 (Fe) and the resins. The resins are attached on the surface and in between the block MIL-53 (Fe) structures.

The X-ray diffraction patterns for the MIL-53 (Fe), AMIL-53 (Fe) and DMIL-53 (Fe) are illustrated in Fig. 1f. The sharp and clearly resolved X-ray diffraction pattern of the as-synthesized MIL-53 (Fe) provides evidence of the formation of a crystallized MOF structure. The XRD data is in good agreement with previously reported works [37]. A decrease in peak intensities of the composites was observed at $2\theta = 12^\circ$, which indicates an irreversible immobilization. Moreover, no new peak was observed in the powder-XRD pattern of the composite photocatalysts implying no marked changes occur in the crystal structure of the original MOF.

XPS measurements were carried out to investigate the chemical environment of the prepared photocatalysts. High resolution XPS spectra of Fe 2p spectrum of the MIL-53 (Fe) (Fig. 2) shows two main peaks at the binding energies of around 712 eV and 725.9 eV corresponding to $Fe\ 2p_{3/2}$ and $Fe\ 2p_{1/2}$ respectively. These peaks shows a slight shift to the lower binding energies in the spectra of AMIL-53 (Fe) and DMIL-53 (Fe) suggesting an intimate interfacial contact. This slight shift of Fe 2p binding energy may originate from the formed close interfacial contact upon loading the resin powders. This intimate interfacial contact that arise from the interaction of the sulfonyl groups of Amberlite 200 resin to the Fe ion center in the composite MOFs or the positively charged quaternary ammonium groups of Amberlite 900 with the negatively charged surface of the MOFs increases the electron density around Fe ion both result in lowering the binding energy.

The molecular structure of the MOF and composite photocatalysts were verified by using Fourier transform infrared spectroscopy (FT-IR), respectively (see Fig. 3). The broad band centered at $2700\ cm^{-1}$ in the spectrum of H_2BDC , assigned to $\nu_{(O-H)}$ stretching, shifts to $3300\ cm^{-1}$ due to metal incorporation in MIL-53 (Fe). The infrared absorption spectrum of MIL-53 (Fe) is in a close agreement to those of reported data in the literature [37]. The zone, below $1300\ cm^{-1}$, shows various bands assigned to the vibrations of H_2BDC ligand. Peaks at $746\ cm^{-1}$ and $533\ cm^{-1}$ correspond to C–H bonding vibrations of the benzene ring and the formation of a metal-oxo bond between the carboxylic group of terephthalic acid and Fe (III) ions. The zone between 1300 and $1700\ cm^{-1}$ is related to the carboxylate ligand and is thus indicative of the coordination of H_2BDC to the iron sites. The two sharp peaks in the spectrum of MIL-53 (Fe) at 1540 and $1380\ cm^{-1}$ are assigned to asymmetric ($\nu_{as}(C-O)$) and symmetric ($\nu_s(C-O)$) vibrations of carboxyl groups, respectively, confirming the presence of the dicarboxylate linker. The band shift of the carboxyl groups of the pure ligand from $1673\ cm^{-1}$ to $1540\ cm^{-1}$ indicates the absence of free ligands in the as-synthesized MIL-53(Fe). Therefore, the FT-IR spectra clearly confirm the formation of MIL-53(Fe) structure.

A comparison of the infrared spectrum of the composites AMIL-53(Fe) and DMIL-53(Fe) with the bare MIL-53 (Fe) (Fig. 3) shows typical absorptions frequencies of the MIL-53 (Fe) (1540 , 1380 , 746 and $533\ cm^{-1}$), which indicates that immobilization was carried out without appreciable changes in the original MOF structure.

3.2. Photocatalytic reactivity

The degradation of two cationic dyes (RhB and MB) and two anionic dyes (SRB and Org II) were analyzed to evaluate and compare the catalytic performance of different systems, where control experiments were conducted (Fig. S1) to compare the removal efficiencies of dyes by various processes with initial dye concentration of $3.3\ mmol\ L^{-1}$.

The adsorption amount of dyes in water solution by MIL-53 (Fe), AMIL-53 (Fe) and DMIL-53 (Fe) before the photocatalytic degradation are summarized in Table 1. Cationic dye RhB was highly adsorbed (21%) by MIL-53 (Fe) compared to the anionic dye SRB

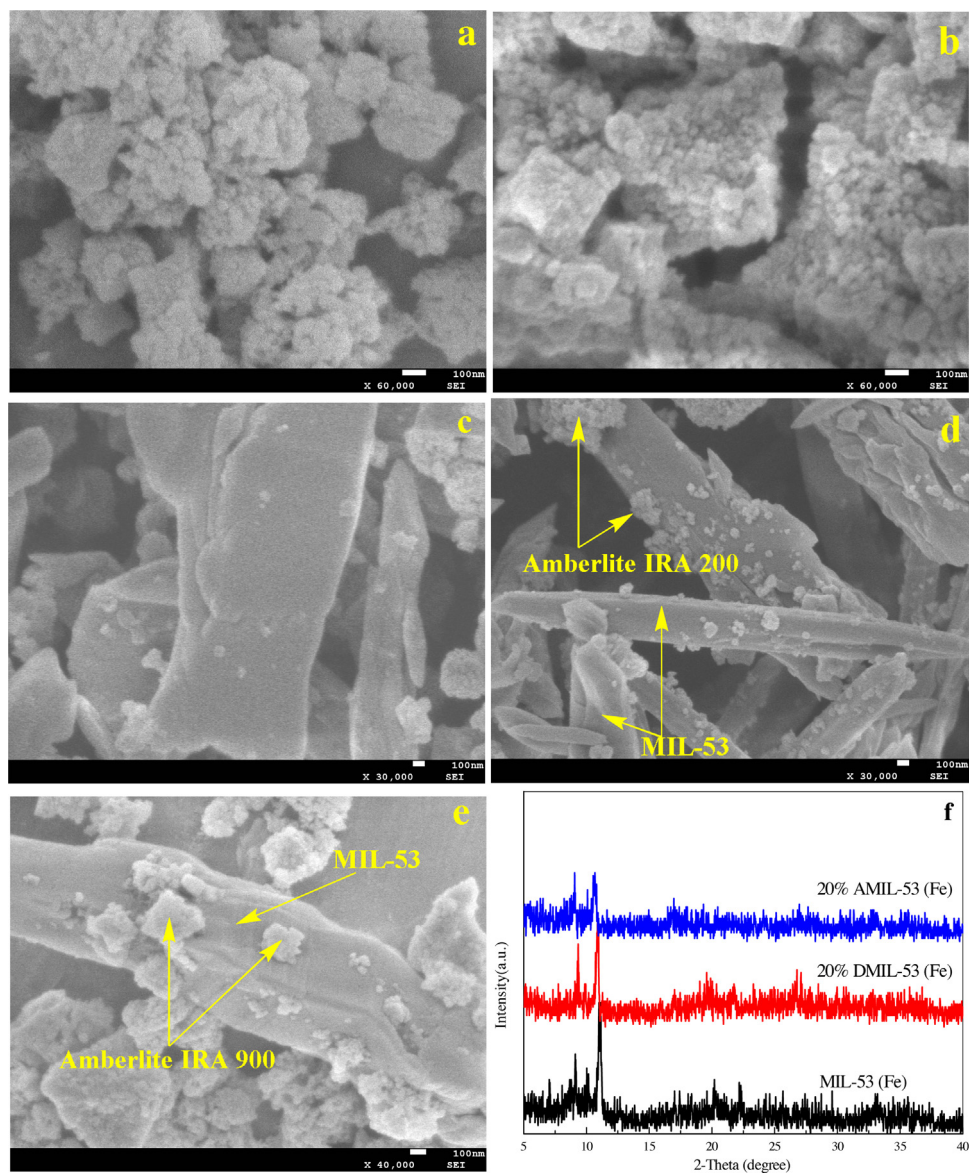


Fig. 1. SEM images of (a) Amberlite IRA-200 (b) Amberlite IRA-900 and (c) MIL-53 (Fe), (d) 20% AMIL-53 (Fe), (e) 20% DMIL-53 (Fe) and (f) XRD patterns of MIL-53 (Fe), 20% DMIL-53 (Fe) and 20% AMIL-53 (Fe).

Table 1

The adsorption amount of dyes on pure and resin-immobilized MIL-53 (Fe) solid powders.

Samples	C_i (mmol/L)	$C_{MIL-53(Fe)}$ (mmol/L)	$C_{AMIL-53(Fe)}$ (mmol/L)	$C_{DMIL-53(Fe)}$ (mmol/L)
RhB	3.3	2.6 (21.1%)	1.7 (47.6%)	2.5 (21.8%)
SRB	3.3	3.15 (4.5%)	2.9 (11.5%)	2.1 (38.4%)

C_i : initial concentration; $C_{MIL-53(Fe)}$: the concentration of dye after adsorption on MIL-53(Fe); $C_{AMIL-53(Fe)}$: the concentration after adsorption on AMIL-53 (Fe); $C_{DMIL-53(Fe)}$: the concentration after adsorption on DMIL-53 (Fe). Note: Figures in brackets denote the percentage of adsorption of total dye concentration. [catalyst] = 0.17 g L⁻¹, pH = 7, $C_i = 3.3 \times 10^{-3}$ M.

(4.5%). This is attributed to the negatively charged surface of MIL-53(Fe) MOF resulted from the carboxyl group rich ligand. However, the adsorption of anionic dye SRB was significantly increased to 38.4% on DMIL-53 (Fe) due to Amberlite IRA 900 immobilization. On the other hand, the capacity of adsorption for cationic dyes, RhB and MB, was also improved after loading Amberlite IRA 200 on

MIL-53(Fe), AMIL-53 (Fe). In contrast, AMIL-53(Fe) doesn't favor adsorption of anionic dyes, SRB and Org II. Similarly, DMIL-53 (Fe) also shows low adsorption for the cationic dyes RhB and MB. Apparently the two photocatalysts have opposite selectivity of adsorption in water. For the photocatalytic degradation (PCD) of different dye pollutants in water, MIL-53(Fe) itself was suspended in water as photocatalyst and showed so radically distinct preference between degradation of cationic dye RhB and anionic dye SRB, preferring to degrade the cationic dyes (Fig. 4). This is in agreement with its adsorption capacity for different dyes in water. Consequently, the PCD of the cationic and anionic dyes was significantly enhanced after modification of MIL-53 (Fe) by Amberlite IRA 200 and Amberlite IRA 900 respectively (Fig. 4). After visible light irradiation for 120 min, no significant degradation of dyes in the absence of the catalyst or light was observed (Fig. S1) indicating the dyes were stable under visible light irradiation alone.

Furthermore, simple mixing of MIL-53 (Fe) with either of the resins does not enhance the PCD of the dyes (Table 2) reflecting immobilization improved the photocatalytic activity rather

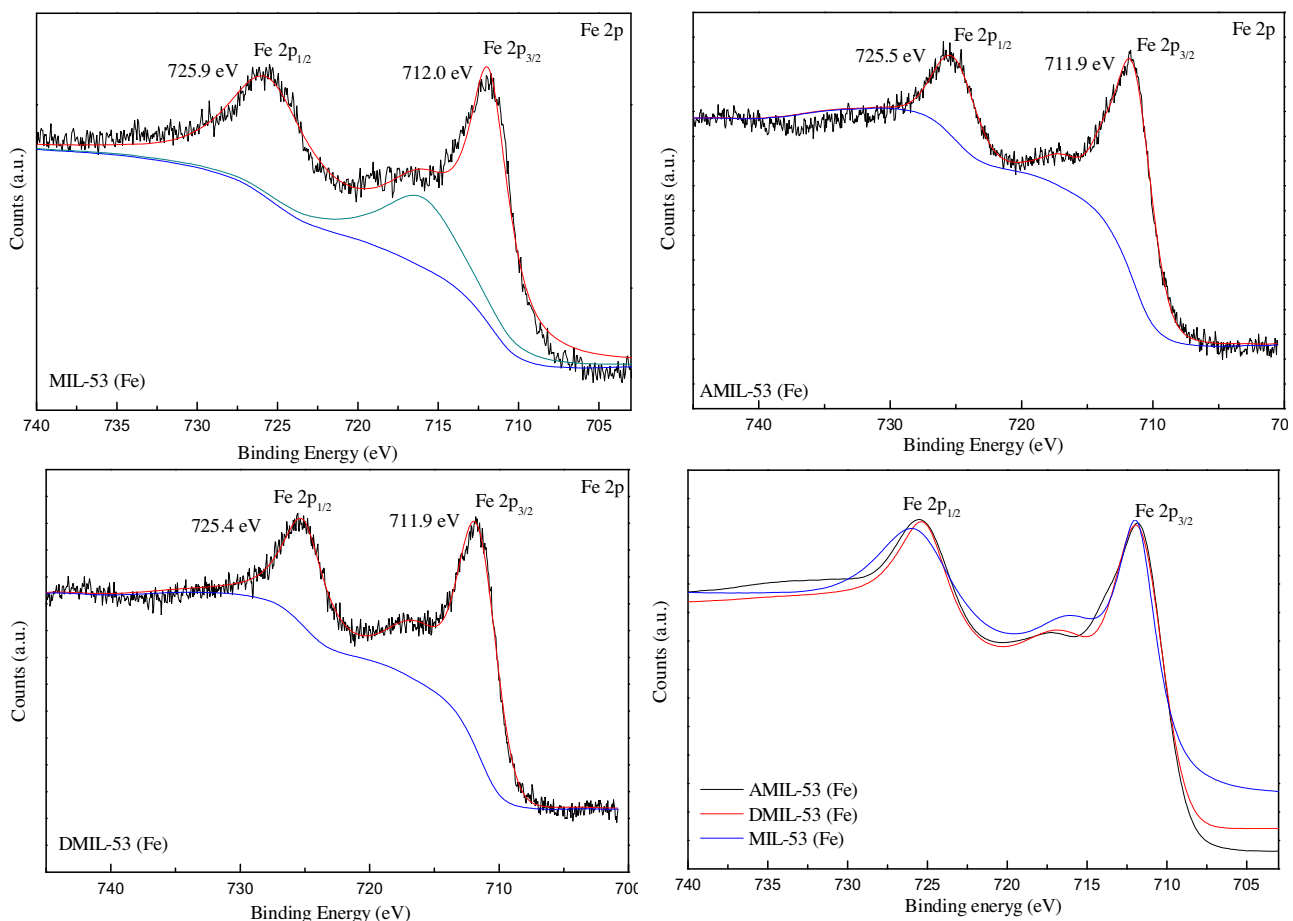


Fig. 2. Fe 2p X-ray photoelectron spectroscopy (XPS) spectra of (a) MIL-53 (Fe) (b) AMIL-53 (Fe) (c) DMIL-53 (Fe) (d) comparison of the Fe 2p XPS spectra of the original and immobilized catalysts.

Table 2

Adsorption and photocatalytic degradation of SRB(A) and RhB(B) over immobilized and mixed catalysts.

(A) SRB	Amberlite IRA-900	DMIL-53 (Fe)	MIL-53 (Fe)	Amberlite IRA-900 (10%) + MIL-53 (Fe) (90%) (simple mixing)
Percent Adsorption	62%	39.3%	5%	56.5%
Percent PCD	18%	96%	24%	35%
(B) RhB	Amberlite IRA-200	AMIL-53 (Fe)	MIL-53 (Fe)	Amberlite IRA-200(10%) + MIL-53 (Fe) (90%) (simple mixing)
Percent Adsorption	68%	47%	22%	64%
Percent PCD	3%	97%	85.4%	61%

[Catalyst] = 0.17 g L⁻¹, pH = 7, C_i = 3.3 × 10⁻³ M, 120 min visible light irradiation.

than the simple existence of the resin. Even though the adsorption capacities were comparable, the effect of immobilization was easily noticeable during the PCD of the dyes. The PCD of RhB and SRB was highly enhanced on the immobilized composites while simple mixing of the MOF and the resins themselves show no appreciable enhancement in the PCD of the dye molecules. More significantly improvement of PCD efficiency was observed for degradation of SRB over DMIL-53(Fe) than MIL-53(Fe) (from $k = 0.01$ to 0.026 min^{-1}). Similarly PCD efficiency for degradation of RhB was enhanced when MIL-53(Fe) is replaced by AMIL-53 (Fe) (from $k = 0.034$ to 0.047 min^{-1}). It is observed that immobilization of Amberlite enhances the PCD to the optimal level by improving the adsorption capacity, which may allow the pollutants to be in close vicinity with the MOF surface generated active species during light irradiation which lead to the degradation of pollutants.

3.3. Photocatalytic priorities

As discussed in the above section the rate of PCD was dependent on the adsorption pattern. The adsorption was obviously determined by the charge interaction of the substrate and the catalyst surface. The resin modified MIL-53 (Fe) composites show charge based degradation preference. The adsorption and degradation of cationic dyes RhB and MB were enhanced after MIL-53 (Fe) was modified with the anionic resin Amberlite IRA 200 (Fig. S2), while degradation of anionic dyes SRB and Org II was highly enhanced after MIL-53 (Fe) was modified with cationic resin Amberlite IRA900. The effect of immobilization was more noticeable during the degradation of anionic dyes and the degradation of SRB was enhanced by 84% over DMIL-53 (Fe) (from $k = 0.01$ to 0.026 min^{-1}) (Figs. 4 and Fig. S2). The surface charge of the composite photo-

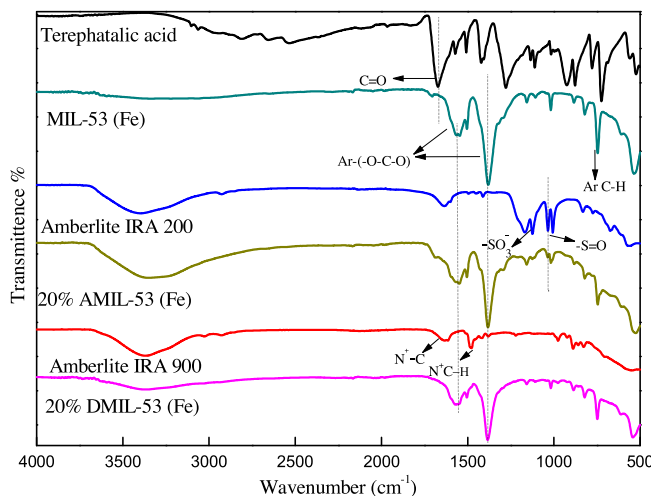


Fig. 3. FT-IR spectra of original and immobilized MIL-53 (Fe).

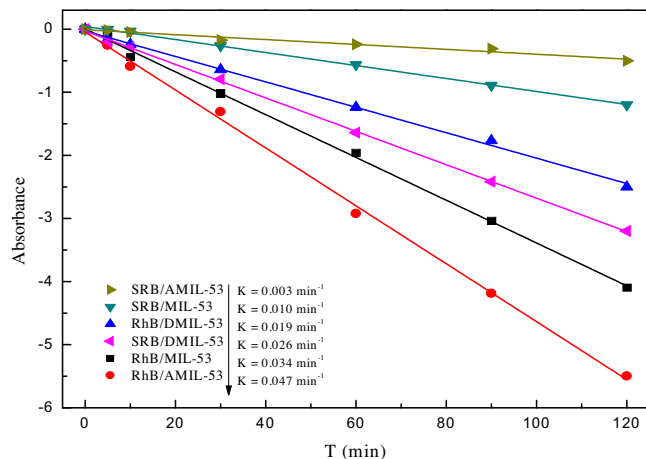


Fig. 4. Photocatalytic degradation of RhB and SRB over MIL-53 (Fe), 20% AMIL-53 (Fe) and 20% DMIL-53 (Fe) [catalyst] = 0.17 g L $^{-1}$, pH = 7, C_i = 3.3×10^{-3} M.

catalysts was monitored to further understand the origin of the observed degradation preference. The zeta potential of 20% AMIL-53 (Fe) and 20% DMIL-53 (Fe) were measured to be -24 mV and $+2$ mV respectively. These values changed after adsorption of dyes by the catalysts. After adsorption of RhB ($\zeta_{\text{RhB}} = 1.06$ mV) the zeta potential of AMIL-53 (Fe) was changed to -1 mV while that of DMIL-53 (Fe) was changed to $+0.5$ mV after adsorption of SRB ($\zeta_{\text{SRB}} = -2.54$ mV). These changes in the surface charge of the composite photocatalysts suggest the adsorption of substrates is due to columbic interaction.

3.4. Substrate dependent tunable degradation

To induce tunable degradation order and evaluate its efficiency, the PCD of dye molecules was further explored by using composite photocatalysts with varying resin/MOF ratio. As shown in Fig. 5, the degradation activity of the catalyst was tuned by altering the ratio of resin to MIL-53(Fe) MOF. PCD of SRB over DMIL-53 (Fe) with different MOF/resin ratio was selected to evaluate the tunable degradation preference of the system. An increase in the percentage of resin loaded apparently increases the adsorption of SRB. This was in agreement with the observed change in the zeta potential of the composites. The zeta potential of the composites were -5 mV, $+0.45$ mV, $+2$ mV, $+12.9$ mV and $+21.3$ mV for the 0% , 10% , 20% , 30% and 40% resin loading respectively. Likewise the PCD of SRB

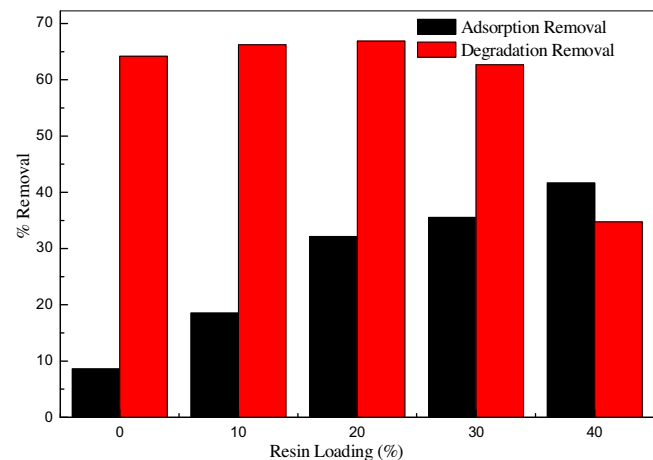


Fig. 5. Adsorption and degradation removal of SRB over DMIL-100 with different Amberlite IRA 900 loading percentage during immobilization (0%, 10%, 20%, 30% and 40%). [catalyst] = 0.17 g L^{-1} , pH = 7, C_i = 3.3×10^{-3} M.

Table 3

The rate constant K for the degradation of SRB over DMIL-53 (Fe) with varying Amberlite IRA-900 to MIL-53(Fe) MOF ratio.

	10%DMIL-53 (Fe)	20%DMIL-53 (Fe)	30%DMIL-53 (Fe)	40%DMIL-53 (Fe)
K_{MB} (min^{-1})	0.0119	0.0098	0.0079	0.0028
K_{SRB} (min^{-1})	0.015	0.014	0.018	0.008
$K_{\text{SRB}}/K_{\text{MB}}$	1.25	1.4	2.25	2.8

[Catalyst] = 0.17 g L^{-1} , pH = 7, C_i = 3.3×10^{-3} M.

increases but excess amount of resin loading beyond the optimal level prevents light penetration which consequently suppresses the photocatalytic degradation. The optimal modified amount of DMIL-53 (Fe) is about 20%, and its apparent rate constant k for the photocatalytic degradation of SRB is 0.032 min^{-1} ; about 3 times that of MIL-53 (Fe) without loading resin. The above results indicate that the observed degradation preference can be further tuned by controlling the resin/MOF ratio during immobilization.

Since a real waste water can not only contain a single component, the degradation order of catalyst towards pollutant substrates in water, efficiency and industrial application were investigated over a simulated solution prepared by mixing MB and SRB which bear opposite charges in water solution. As shown in Fig. 6a the absorption peak of MB at 670 nm was lowered faster (84%) compared to that of SRB (11%) at 554 nm during the PCD of the mixed solution over AMIL-53 (Fe) indicating the composite photocatalyst can selectively and efficiently degrade cationic dye in the model wastewater treatment. In contrast the photodegradation of SRB was enhanced when DMIL-53 (Fe) was utilized as a photocatalyst with 73% removal compared to 59% MB (Fig. 6b). More interestingly, the selectivity of the composite photocatalyst can be enhanced by controlling the resin/MOF ratio. Apparently, increasing resin percentage in the composite photocatalyst increases the ability to choose and degrade certain dyes preferentially than others (Table 3), which could be due to the columbic attraction and repulsion forces experienced by the dye molecules.

3.5. Possible photocatalytic pathway

Photoelectrochemical experiments were conducted to understand the effect of immobilization on the optical absorption, charge carrier transfer. As can be seen in Fig. 7a, the pure organic linker (H_2BDC) does not absorb any visible light indicating direct excitation of iron-oxo complex cluster is the main contributor for

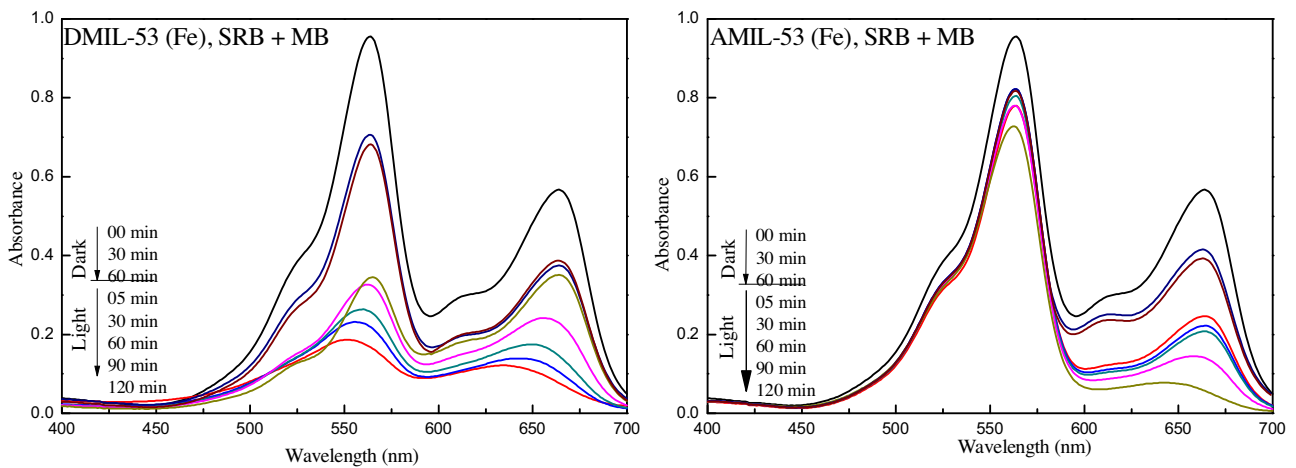


Fig. 6. Temporal UV-vis absorption spectral change during the photocatalytic degradation of mixed solution of SRB and MB over (right) 20% AMIL-53 (Fe) and (left) 20% DMIL-53 (Fe). [catalyst] = 0.17 g L⁻¹, pH = 7, C_{SRB} = 3.3 × 10⁻³ M, C_{MB} = 3.3 × 10⁻³ M. Every filtrate sample was diluted with water by three-fold before determination by UV-vis spectrophotometer.

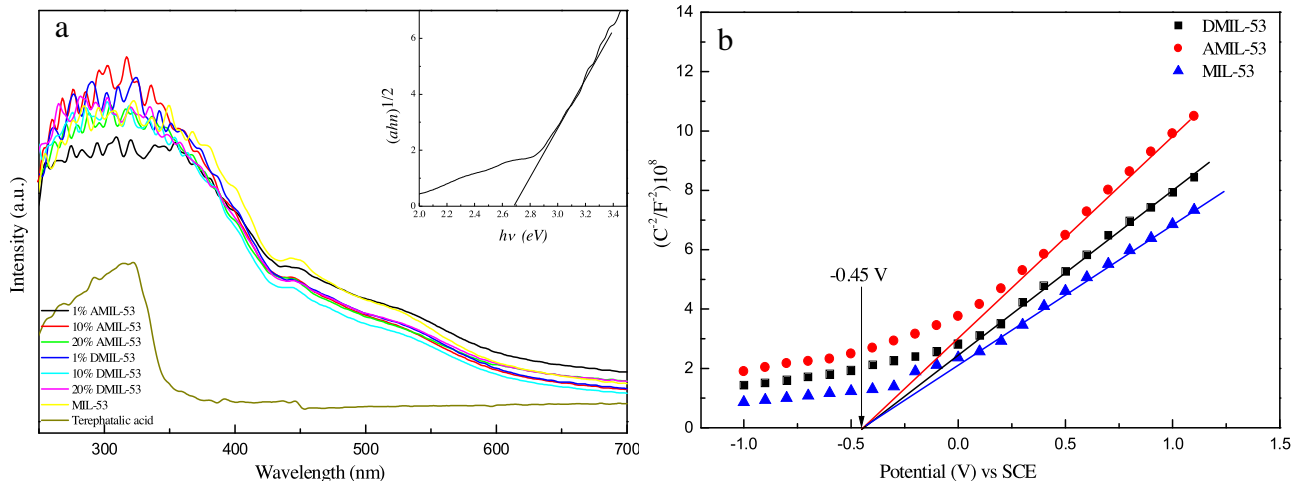


Fig. 7. (a) UV-vis spectrum of MIL-53 (Fe), AMIL-53 (Fe), DMIL-53 (Fe) and Terephthalic acid (inset a), optical band gap obtained from the plots of $(\alpha h\nu)^{1/2}$ versus the photon energy ($h\nu$) of MIL-53 (Fe) (b), Typical Mott-Schottky plots of MIL-53 (Fe), AMIL-53 (Fe) and DMIL-53 (Fe) in 0.1 M Na₂SO₄ aqueous solution (pH 7).

the photocatalytic performance of MIL-53 (Fe). The tested samples show strong absorption band in the range of 200–500 nm which correspond to the ligand-to-metal charge transfer(LMCT) and intraligand n-π and π- π transitions [34,36]. In addition, UV-vis DRS spectra of the as-prepared composites are similar to that of original MIL-53 (Fe) indicating the light harvesting ability of the samples is mainly due to the MIL-53(Fe) MOF. To further understand the source of light harvesting ability, flat band potential of the bare and resin-immobilized photocatalysts was obtained from the Mott-Schottky plot. As depicted in Fig. 6c the flat band potential of the three catalysts obtained in 0.1 M Na₂SO₄ solution at 1000 kHz lie at a single point indicating immobilization does not alter the electronic properties of the MIL-53(Fe) and the optical properties of the composite mainly depends on the original MIL-53(Fe) particles. In addition, UV-vis DRS spectrum of the MIL-53(Fe) MOF indicates the onset of the main absorption edge of is located at 480 nm. The band gap was estimated from a plot of the transformed Kubelka-Munk function versus the energy of absorbed light (Fig. 7a inset) from which the optical band gap was calculated to be 2.75 eV. Furthermore, as can be seen from Fig. 7b, the linear slope for $1/C^2$ vs Potential curve is positive suggesting the MOF MIL-53(Fe) is an n-type semiconductor. The flat band potential of MIL-53(Fe) obtained by extrapolation of Mott-Schottky plot indicates -0.45 V vs SCE at

pH 7, corresponding to ca. -0.22 V vs NHE. As indicated by Yang et al. [17], the conduction band potential (E_{CB}) of the n-type semiconductor is located 0.1 V above the flat band potential (E_{fb}). So the conduction band of MIL-53 (Fe) is ca. -0.32 V vs NHE. Furthermore, the valence band potential can be calculated from the empirical equation $E_{vb} = E_g + E_{cb}$, where E_{vb} is the valence band potential, E_{cb} is the conduction band potential and E_g is the band gap energy of the semiconductor. Correspondingly, the valence band potential was calculated at about 2.43 eV.

To further understand the advantage of resin immobilization in improving the charge carrier transfer, electrochemical impedance spectra (EIS) Nyquist plot for different loading ratio of resin was performed. As shown in Fig. 8, 10% and 20% both DMIL-53 (Fe) and AMIL-53 (Fe) display the smaller radius of curvature than that bare MIL-53(Fe), indicating that there is indeed an optimum loading percentage range of Amberlite resin components for the improvement of the charge carrier transfer behavior of the original MIL-53 (Fe).

Specific quenching agents were employed to verify the dominant active species in the photocatalytic degradation of dyes over MIL-53(Fe) MOF under visible-light irradiation. Benzoquinone (BQ) for superoxide radical (O₂^{·-}), sodium azide (Na₃N) for the singlet oxygen (¹O₂), ammonium oxalate (NH₄C₂O₄) for photo-generated holes (h_{vb}^+). As shown in Fig. 9, after 120 min of visible light irradi-

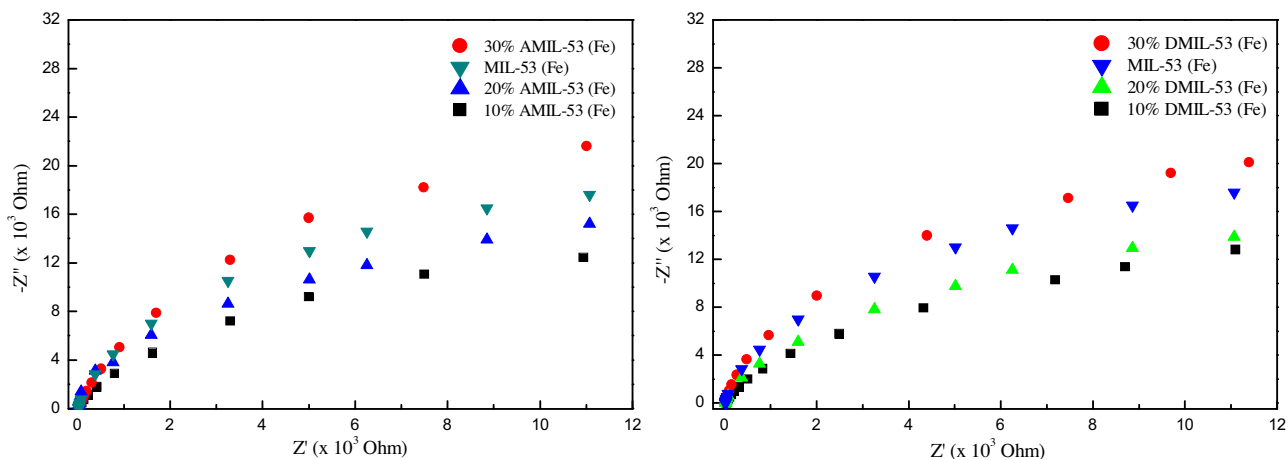


Fig. 8. Nyquist impedance plots of AMIL-53 (Fe) (left) and DMIL-53 (Fe) (right) composites.

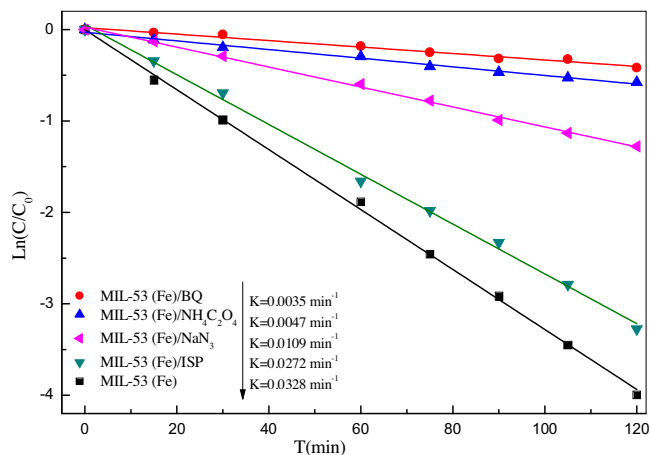


Fig. 9. Effect of scavengers on the photocatalytic degradation of RhB over MIL-53 under visible light irradiation [catalyst] = 0.17 g L⁻¹, pH = 7, $C_{\text{RhB}} = 3.3 \times 10^{-3}$ M.

ation, the degradation rate constant declined from 0.032 min^{-1} to 0.011 min^{-1} , 0.0047 min^{-1} and 0.0035 min^{-1} due to the addition of NaN_3 , $\text{NH}_4\text{C}_2\text{O}_4$ and BQ respectively suggesting photogenerated holes and superoxide radicals are the main active species for the degradation of dye molecules.

This is in agreement with the band gap values of the MOF and the redox potential of the dyes. Since the valence band (VB) of MIL-53 (Fe) (2.43 V vs. NHE) is higher than the redox potential of $\cdot\text{OH}/\text{OH}^-$ (2.38 V vs. NHE), formation of hydroxyl radical is possible. Furthermore, terephthalic acid was employed as a probe molecule to quench hydroxyl radicals and the resulting highly fluorescent product, 2-hydroxyterephthalic acid ($\lambda_{\text{exc}} = 315 \text{ nm}$, $\lambda_{\text{em}} = 425 \text{ nm}$), was detected to confirm the generation of hydroxyl radicals. As shown in Fig. S3, the maximum peak intensity centered at 425 nm affirms the formation of hydroxyl radicals. The redox potential of dyes such as RhB and MB is significantly lower than VB level of AMIL-53 (Fe), suggesting that direct hole oxidation process is also energetically favorable.

3.6. Stability and recyclability

MOFs stability and reusability are affected by the leaching of the metal ion from the framework into the solution. The concentration of iron ions in the supernatant of the composite solution was detected by using the colorimetric method and the results are presented in Fig. 10. The result clearly shows iron (III) ion leaching

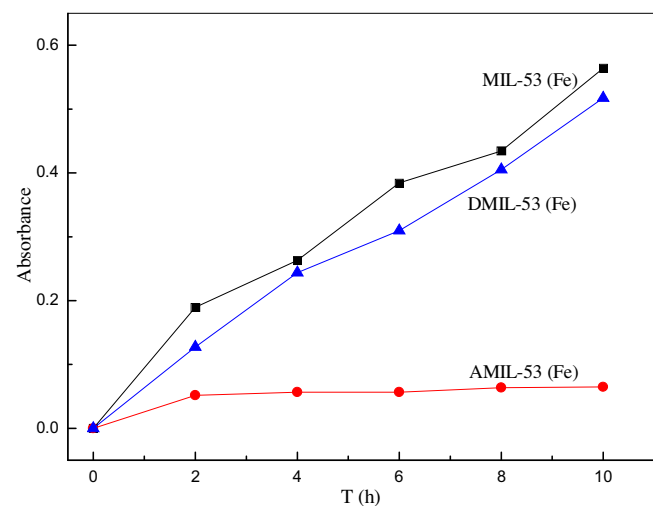


Fig. 10. Colorimetric detection of leached Fe (III) ion from MIL-53 (Fe), 20% AMIL-53 (Fe) and 20% DMIL-53(Fe) in water under visible light irradiation.

Table 4
RhB removal over recycled MIL-53(Fe), 20% DMIL-53 (Fe) and 20% AMIL-53 (Fe).

	MIL-53 (Fe)	DMIL-53 (Fe)	AMIL-53 (Fe)
1st run	95%	91%	95.5%
2nd run	62%	90%	94.1%
3rd run	16%	86%	93.7%
4th run	—	80%	93.2%
5th run	—	60%	91.5%

is significantly reduced by the immobilization of Amberlite IRA 200 over MIL-53 (Fe). Compared to that of MIL-53 (Fe) and DMIL-53 (Fe), the appreciable leaching reduction from AMIL-53 (Fe) is attributed to the chelation formed between sulphonate group of Amberlite IRA 200 and the metal ion. To investigate the reusability, the photocatalysts were recovered by filtration, washed with ethanol and water to completely remove the absorbed dyes on the surface of catalyst and vacuum dried before reusing. As shown in Table 4, compared to that of MIL-53 (Fe), both AMIL-53 (Fe) and DMIL-53 (Fe) show an improved performance with less significant loss of activity after 5 cycles.

Accordingly, a possible mechanism for the tunable PCD of hazardous organics over MIL-53(Fe)-resin composites is proposed. As shown in Fig. 11, cationic dyes are preferentially adsorbed by AMIL-53 due to the negative surface charge of both carboxyl lig-

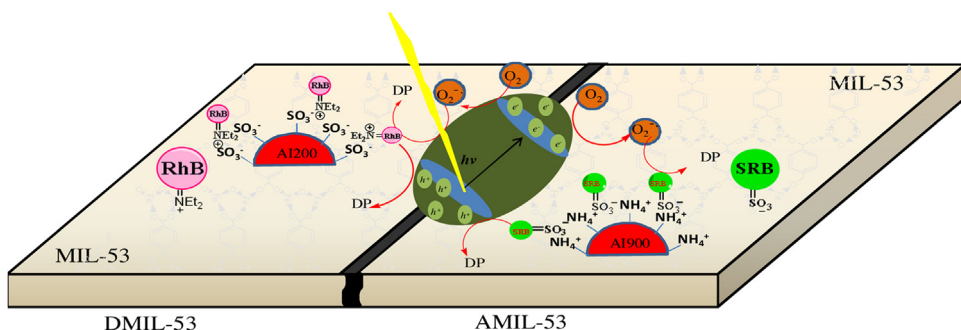


Fig. 11. A schematic illustration of photocatalytic degradation of cationic and anionic dyes over AMIL-53 (Fe) and DMIL-53 (Fe) under visible-light irradiation (AI900: Amberlite IRA 900, AI200: Amberlite IRA 200, DP: degradation products).

and of MIL-53(Fe) and Amberlite IRA-200, while anionic dyes are preferentially adsorbed by DMIL-53 due to the presence of Amberlite IRA-900. Under visible-light irradiation, the composites are excited and photogenerated electrons/holes with strong degradation capacity migrate to the catalyst surface and preferentially degrade organic pollutants adsorbed by the composites.

4. Conclusion

In general, a series of loaded-resin MIL-53 (Fe) composites have been fabricated and result a cationic and anionic composites depending on the type of resin utilized during the immobilization process. Simple mechanical mixing of the resin and the MOF show no significant improvement in the PCD of dyes compared to the immobilized photocatalyst, indicating an efficient interfacial contact is responsible for the improvement of the PCD. The investigated dyes show charge based adsorption leading to a selective photodegradation. Dye adsorption was altered by controlling resin/MOF ratio. Higher percentages of resins improve adsorption capacity but excess amount of the resin beyond the optimal level (20% AMIL-53 (Fe) and 20%DMIL-53 (Fe)) reduces light penetration resulting in reduced PCD performance. Controlling the surface charge of the catalyst through immobilization of resin allows tuning the catalyst preference to degrade the desired kind of pollutants. In addition, the recyclability of the original MIL-53 (Fe) was improved after immobilization. Especially, immobilization of Amberlite IRA 200 significantly reduces iron (III) ion leaching leading to an improved stability and recyclability. Considering the numerous numbers of resins, this work offers an insight in utilizing resins as loaded role rather than traditional supports to improve the degradation preference, catalytic activity, stability, and optical properties of photocatalysts.

Acknowledgements

This work was supported by the National Natural Science Foundation of China (21377067, 21407092, 21577077, 21577078, 21677086) and the Natural Science Foundation for Innovation Group of Hubei Province, China (2015CFA021).

Appendix A. Supplementary data

Supplementary data associated with this article can be found, in the online version, at <http://dx.doi.org/10.1016/j.apcatb.2016.10.072>.

References

- [1] R. Liang, R. Chen, F. Jing, N. Qina, L. Wu, Multifunctional polyoxometalates encapsulated in MIL-100(Fe): highly efficient photocatalysts for selective transformation under visible light, *Dalton Trans.* 44 (2015) 18227–18236.
- [2] M. Ji, X. Lan, Z. Han, C. Hao, J. Qiu, Luminescent properties of metal-organic framework MOF-5: relativistic time-dependent density functional theory investigations, *Inorg. Chem.* 51 (2012) 12389–12394.
- [3] T. Araya, S. Quan, J. Man-ke, M. Wan-hong, D. Johnson, H. Ying-ping, Selective photocatalytic degradation of organic pollutants using a water-insoluble Zn-schiff base complex, *Water Air Soil Pollut.* 227 (2016) 284.
- [4] K.G.M. Laurier, F. Verwoortele, R. Ameloot, D.E. De Vos, J. Hofkens, M.B.J. Roeffaers, Iron(III)-based metal-organic frameworks as visible light photocatalysts, *J. Am. Chem. Soc.* 135 (2013) 14488–14491.
- [5] P. Küsgens, M. Rose, I. Senkovska, H. Fröde, A. Henschel, S. Siegle, S. Kaskel, Characterization of metal-organic frameworks by water adsorption, *Microporous Mesoporous Mater.* 120 (2009) 325–330.
- [6] J. Li, W. Ma, Y. Huang, X. Tao, J. Zhao, Y. Xu, Oxidative degradation of organic pollutants utilizing molecular oxygen and visible light over a supported catalyst of Fe(bpy)₃²⁺ in water, *Appl. Catal. B: Environ.* 48 (2004) 17–24.
- [7] X. Liu, P. Lv, G. Yao, C. Ma, Y. Tang, Y. Wu, P. Huo, J. Pan, W. Shi, Y. Yan, Selective degradation of ciprofloxacin with modified NaCl/TiO₂ photocatalyst by surface molecular imprinted technology, *Colloids Surf. A: Physicochem. Eng. Aspects* 441 (2014) 420–426.
- [8] E. Haque, J.E. Lee, I.T. Jang, Y.K. Hwang, J. Chang, J. Jegal, S.H. Jhung, Adsorptive removal of methyl orange from aqueous solution with metal-organic frameworks, porous chromium-benzenedicarboxylates, *J. Hazard. Mater.* 181 (2010) 535–542.
- [9] Z. Hasan, S.H. Jhung, Removal of hazardous organics from water using metal-organic frameworks (MOFs): plausible mechanisms for selective adsorptions, *J. Hazard. Mater.* 283 (2015) 329–339.
- [10] J.E. Warren, C.G. Perkins, K.E. Jelfs, P. Boldrin, P.A. Chater, G.J. Miller, T.D. Manning, M.E. Briggs, K.C. Stylianou, J.B. Claridge, M.J. Rosseinsky, Shape selectivity by guest-driven restructuring of a porous material, *Angew. Chem. Int. Ed.* 53 (2014) 4592–4596.
- [11] R. Matsuda, Selectivity from flexibility, *Nature* 509 (2014) 434.
- [12] X. Zhao, X. Bu, T. Wu, S. Zheng, L. Wang, P. Feng, Selective anion exchange with nanogated isoreticular positive metal-organic frameworks, *Nat. Commun.* 4 (2013) 2344.
- [13] J. Sun, P. Yan, G. An, J. Sha, G. Li, G. Yang, Immobilization of polyoxometalate in the metal-organic framework rht-MOF-1: towards a highly effective heterogeneous catalyst and dye scavenger, *Sci. Rep.* 6 (2016) 25595.
- [14] F. Cacho-Bailo, S. Catalán-Aguirre, M. Etxeberria-Benavides, O. Karvanb, V. Sebastian, C. Téllez, J. Coronas, Metal-organic framework membranes on the inner-side of a polymeric hollow fiber by microfluidic synthesis, *J. Memb. Sci.* 476 (2015) 277–285.
- [15] L. Yue, J. Guo, Q. Yang, X. Luo, J. Lian, J. Yang, L. Wang, Biotemplate synthesis of mesoporous iron phosphomolybdate supported on silica with enhanced photocatalytic property, *Mater. Lett.* 157 (2015) 225–227.
- [16] C. Petit, T.J. Bandosz, MOF-graphite oxide composites: combining the uniqueness of graphene layers and metal-organic frameworks, *Adv. Mater.* 21 (2009) 4753.
- [17] Z. Yang, X. Xu, X.X. Liang, C. Lei, Y. Wei, P. He, B. Lv, H. Ma, Z. Le, MIL-53(Fe)-graphene nanocomposites: efficient visible-light photocatalysts for the selective oxidation of alcohols, *Appl. Catal. B: Environ.* 198 (2016) 112–123.
- [18] R. Liang, L. Shen, F. Jing, N. Qin, L. Wu, Preparation of MIL-53(Fe)-reduced graphene oxide nanocomposites by a simple self-assembly strategy for increasing interfacial contact: efficient visible-light photocatalysts, *ACS Appl. Mater. Interfaces* 7 (2015) 9507–9515.
- [19] P. Sun, R. Ma, W. Ma, J. Wu, K. Wang, T. Sasaki, H. Zhu, Highly selective charge-guided ion transport through a hybrid membrane consisting of anionic graphene oxide and cationic hydroxide nanosheet superlattice units, *NPG Asia Mater.* 8 (2016) 1–10.
- [20] Y. Monguchia, T. Ichikawa, K. Nozaki, K. Kihara, Y. Miyake, Y. Sawama, H. Sajiki, Development of chelate resin-supported palladium catalysts for chemoselective hydrogenation, *Tetrahedron* 71 (2015) 6499–6505.
- [21] M. Kuzminska, R. Backov, E.M. Gaigneaux, Behavior of cation-exchange resins employed as heterogeneous catalysts for esterification of oleic acid with trimethylolpropane, *Appl. Catal. A: Gen.* 504 (2015) 11–16.

- [22] Z. Zhu, M. Zhang, F. Liu, C. Shuang, C. Zhu, Y. Zhang, A. Li, Effect of polymeric matrix on the adsorption of reactive dye by anion-exchange resins, *J. Taiwan Inst. Chem. Eng.* 000 (2016) 1–6.
- [23] X. Jiang, J. Huang, Adsorption of rhodamine B on two novel polar-modified post-cross-linked resins: equilibrium and kinetics, *J. Colloid Interface Sci.* 467 (2016) 230–238.
- [24] P.A. Turhanen, J.J. Vepsäläinen, S. Peräniemi, Advanced material and approach for metal ions removal from aqueous solutions, *Sci. Rep.* 5 (2015) 8992.
- [25] E. Marais, T. Nyokong, Adsorption of 4-nitrophenol onto Amberlite IRA-900 modified with metallophthalocyanines, *J. Hazard. Mater.* 152 (2008) 293–301.
- [26] A. Molinari, G. Varani, E. Polo, S. Vaccari, A. Maldotti, Photocatalytic and catalytic activity of heterogenized $W_{10}O_{32}^{4-}$ in the bromide-assisted bromination of arenes and alkenes in the presence of oxygen, *J. Mol. Catal. A: Chem.* 262 (2007) 156–163.
- [27] W. Ma, Y. Huang, J. Li, M. Cheng, W. Song, J. Zhao, An efficient approach for the photodegradation of organic pollutants by immobilized iron ions at neutral pHs, *Chem. Commun.* 13 (2003) 1582–1583.
- [28] G.B. Kunde, G.D. Yadav, Synthesis, characterization and application of iron-aluminate nodules in advanced Fenton's oxidation process, *J. Environ. Chem. Eng.* 3 (2015) 2010–2021.
- [29] M.M. Cheng, W. Ma, Jing Li, Y. Huang, J. Zhao, Visible light assisted degradation of dye pollutants over Fe (III)-loaded resin in the presence of H_2O_2 at neutral pH values, *Environ. Sci. Technol.* 38 (2004) 1569–1575.
- [30] K. Feng, L. Wu, L. Zhang, C. Tung, IRA-200 resin-supported platinum(II) complex for photooxidation of olefins, *Tetrahedron* 63 (2007) 4907–4911.
- [31] R. Liang, F. Jing, L. Shen, N. Qin, L. Wu, MIL-53(Fe) as a highly efficient bifunctional photocatalyst for the simultaneous reduction of Cr(VI) and oxidation of dyes, *J. Hazard. Mater.* 287 (2015) 364–372.
- [32] J. Du, Y. Yuan, J. Su, F. Peng, X. Jiang, L. Qiu, A. Xie, Y. Shen, J. Zhu, New photocatalysts based on MIL-53 metal-organic frameworks for the decolorization of methylene blue dye, *J. Hazard. Mater.* 190 (2011) 945–951.
- [33] L. Ai, L. Li, C. Zhang, J. Fu, J. Jiang, MIL-53(Fe): a metal-organic framework with intrinsic peroxidase-like catalytic activity for colorimetric biosensing, *Chem. Eur. J.* 19 (2013) 15105–15108.
- [34] T. Loiseau, C. Serre, C. Huguenard, F. Gerhard, F. Taulelle, M. Henry, T. Bataille, G. Férey, A rationale for the large breathing of the porous aluminum terephthalate (MIL-53) upon hydration, *Chem. Eur. J.* 10 (2004) 1373–1382.
- [35] P. Horcajada, C. Serre, G. Maurin, N.A. Ramsahye, F. Balas, M.V. Regí, M. Sebban, F. Taulelle, G. Férey, Flexible porous metal-organic frameworks for a controlled drug delivery, *J. Am. Chem. Soc.* 130 (2008) 6774–6780.
- [36] A. Shigematsu, T. Yamada, H. Kitagawa, Wide control of proton conductivity in porous coordination polymers, *J. Am. Chem. Soc.* 133 (2011) 2034–2036.
- [37] L. Ai, C. Zhang, L. Li, J. Jiang, Iron terephthalate metal-organic framework: revealing the effective activation of hydrogen peroxide for the degradation of organic dye under visible light irradiation, *Appl. Catal. B: Environ.* 148–149 (2014) 191–200.